FISFVIER

Contents lists available at ScienceDirect

# Journal of Building Engineering

journal homepage: www.elsevier.com/locate/jobe



Full length article

# Pyrolysis modelling of insulation material in coupled fire-structure simulations

Qingfeng Xu<sup>a</sup>, Hèrm Hofmeyer<sup>a,\*</sup>, Johan Maljaars<sup>a,b</sup>, Ruud A.P. van Herpen<sup>a,c</sup>

- <sup>a</sup> Eindhoven University of Technology, Eindhoven, The Netherlands
- b TNO, Delft, The Netherlands
- <sup>c</sup> Peutz Consulting Engineers, Mook, The Netherlands

#### ARTICLE INFO

# Keywords: Finite element method Pyrolysis Thermomechanical simulations Insulation material Fire-structure simulations

## ABSTRACT

This paper presents a modelling approach to predict the thermodynamical and thermomechanical behaviour of structures with a layer of insulation material under fire, which takes into account the pyrolysis of the insulation and its effects on the structure. First, an existing 1D pyrolysis model is implemented and verified by theoretical and validated by experimental results. Then the model's 1D setup is integrated into 3D Heat Transfer (HT) analyses of structures. The obtained thermodynamical results, i.e. temperatures as a function of time and the pyrolysis process, are transferred to a thermomechanical Structural Response (SR) analysis. Mechanical results are then obtained via temperature and pyrolysis-dependent material properties. The resulting HT and SR analyses are demonstrated in fire-structure simulations of facades made of sandwich panels, including their supporting frames with steel sections, and bolt and screw connections, modelled by non-linear spring elements. It is shown that in a short time window of 100 s, pyrolysis is limited to certain zones of the panel and for limited depths. Nevertheless, due to the endothermic process, it reduces expansion and bending of the panels, and consequently results in smaller displacements, and delayed failure of the connections. For longer periods, with connection failures neglected, significant pyrolysis takes place, which influences the temperature distribution in the complete interior of the sandwich panel. However, this has only a marginal effect on the structural behaviour. In conclusion, pyrolysis effects are relevant, can be modelled, and may somewhat reduce fire risks in structures. Future research can combine pyrolysis with advanced modelling of bolt and screw connections, using a twoscale method. As such, all relevant details of structures can be modelled and investigated for different fire scenarios, including fire-structure effects, all still to be validated by experiments.

## 1. Introduction

As full-scale fire experiments for real-world structures are disproportionately expensive, and inevitably only cover a single case, research on the coupling of realistic fire simulations with structural (i.e. thermomechanical) simulations has seen increasing attention. With these kinds of simulations, different types of structures have been studied, such as building facades, sandwich panels, tall buildings, and tunnels [1–4]. Most related research applies a Computational Fluid Dynamics-Finite Element Model (CFD–FEM) one-way coupled method: the fire is modelled by CFD software to obtain the temperature field on the fire-exposed structural components; the thermomechanical response of the components is subsequently found by a FEM. For example, Luo et al. developed

E-mail address: h.hofmeyer@bwk.tue.nl (H. Hofmeyer).

<sup>\*</sup> Corresponding author.

simulations for predicting the thermomechanical damage of glass-reinforced polymer composite materials subjected to fire [5]. For every time increment in their simulation, data was transferred between the CFD and FEM domain, which led to an accurate prediction of the behaviour of the sandwich panel compared to an experiment. Key et al. applied a multi-continuum theory to predict the progressive failure of composite materials [6]. They used a one-way coupled CFD–FEM method, since the fire behaviour was described by a one-dimensional heat diffusion equation, and was not affected by structural or material failure. However, it may be relevant to use a two-way coupled CFD–FEM method: Yan and Gernay [7] investigated the behaviour of steel members subjected to localised fires. By comparing simulations and experiments, they found that the simulations yielded more conservative predictions than the experiments if the influence of the structure on the fire was not taken into account.

Frequently used for buildings and structures, a sandwich panel consists of two thin-walled plates, also referred to as faces, and a core. Traditionally, materials like stone wool, polyurethane (PUR), polyisocyanurate (PIR), expanded polystyrene (EPS), and extruded polystyrene (XPS) have been used for the core. Their flammability was investigated by e.g. Giunta d'Albani et al. [8]. With new developments in material science, polymer composites are also increasingly applied to the core, e.g. to increase the core's shear stiffness [9,10]. Most research to date has focused on the mechanical behaviour of sandwich panels, to improve the issues associated with traditional core materials, e.g. termite attacks, water disintegration, mould, and poor penetration resistance against wind-borne debris [11]. Although composite materials may improve some of these properties, both traditional and new core materials provide risks during a fire. For example, Khan et al. found that typical flame-retardant aluminium composite panels could be ignited at a lower heat flux compared to traditional panels [12]. As a panel's core is often not directly exposed to the air, pyrolysis may take place, the chemical decomposition of material at high temperatures without oxygen. Birman et al. concluded that it is necessary to account for the process of resin decomposition, a precursor or part of pyrolysis, as this may significantly affect the strength of the panels [13]. Several approaches have been studied for modelling pyrolysis. Hostikka suggests that the pyrolysis model should be kept as simple as possible, as a first-order single-step reaction scheme provides reasonable predictions for the heat release rate [14]. Relevant here, and using a one-dimensional analytical model, Thi et al. developed a user-defined subroutine UMATHT in finite element programme Abaqus, to predict the temperature distribution of timber exposed to fire [15]. Their thermodynamic and thermomechanical material properties were based on experiments.

Due to pyrolysis, the core material degrades and partly becomes a gaseous product, and so thermal and mechanical material properties change. As such, pyrolysis needs to be taken into account in a Heat Transfer (HT) analysis, which makes use of the thermal material properties. Henderson et al. proposed a mathematical model to predict the thermal response of pyrolysis, and this model was later validated by an experiment [16,17]. Their results show that accurate HT simulations can be carried out if the material's kinematic and thermal properties are defined well. Zhang implemented Henderson's model to simulate the thermomechanical behaviour of Polymer Matrix Composites (PMC) [18], and similar efforts were carried out by Li et al. [19]. The good agreement obtained shows the capability of the model to predict pyrolysis behaviour for different materials. Whereas the previous two projects applied commercial finite element programmes, Summers et al. developed a finite element approach themselves, and verified thermodynamical outcomes with commercial software [20]. Richter and Rein proposed a pyrolysis and oxidation model for predicting the charring and burning of timber via a multi-scale approach [21]. As mentioned above, accurate kinetic parameters are critical to predicting a pyrolysis reaction, and Li et al. suggested a way to find the possible range of values of the so-called pre-exponential factor, explained later in this article, and activation energy by a genetic algorithm [22].

Numerous research projects have been carried out on pyrolysis, but only a few relate to the explicit modelling of the effects of pyrolysis on the structural, i.e. mechanical behaviour of structures, if at all on the building scale. Some of the most related examples are research on pyrolysis within compressed wood samples [23], the effect of pyrolysis on microstructures [24], and the degradation of timber elements [25].

In summary, the failure prediction of a structure under fire requires that three domains are solved simultaneously: (a) fire dynamics, (b) thermodynamical heat transfer, and (c) thermomechanical structural response. The first domain should provide realistic fire scenarios using CFD; the second domain is used to obtain the time-dependent temperature variation of all relevant structural components; and the third domain determines the nonlinear structural response, e.g. concerning deformations and failure. Innovative building materials and construction techniques introduce more complexities to these domains. The contribution of this paper is to provide fire-structure simulations, on the scale of building structures, with a computationally efficient and easy-to-implement, yet reasonably accurate, model for insulation pyrolysis, to study the effects of pyrolysis on the global scale structure. Specifically, it studies the inclusion of the pyrolysis behaviour of insulation panel core material in coupled fire-structure simulations of sandwich panels. The pyrolysis model is based on an existing 1D model, which is applied for each column of finite elements over the thickness, in 3D HT analyses of structures. Since the degradation of material due to pyrolysis is considered, the thermomechanical Structural Response (SR) analysis is also extended. The resulting HT and SR analyses are demonstrated in both so-called One-Way Coupled (OWC) and Two-Way Coupled (TWC) fire-structure simulations of facades made of sandwich panels. The importance of pyrolysis modelling is evaluated by comparing the results.

In the next section, the pyrolysis model will be presented, both with respect to its theory and finite element implementation, and the principles of coupled fire-structure simulations will be introduced. In Section 3, the pyrolysis model will be verified and validated, first for the existing approach, then for the modified approach as needed for the subsequent fire-structure simulations. In Section 4, details will be given on how the pyrolysis model can be used within fire-structure simulations. Hereafter, in Section 5, a case study will be presented, in which a building facade with several sandwich panels will be studied by OWC and TWC simulations. After a discussion that relates the importance of pyrolysis to the inclusion of structure-to-fire effects, Section 6 is dedicated to conclusions and recommendations for future research. Code and scripts to reproduce all the simulations in this paper are available on GitHub [26].

#### 2. Pyrolysis model, finite element implementation, coupled fire-structure simulations

This section presents some fundamentals by describing (a) an existing pyrolysis model in Section 2.1, (b) its finite element implementation in Section 2.2, and (c) the setup of coupled fire-structure simulations in Section 2.3, which utilises the concept of the Adiabatic Surface Temperature (AST) as introduced by Wickström [27].

#### 2.1. Pyrolysis model

The 1D pyrolysis model as used as a start is based on [16,17]. Assumptions for the model are that (a) there is no thermo-chemical expansion in the solid, i.e. either char or unpyrolysed material; (b) there is no accumulation of decomposition gases in the solid; (c) thermal equilibrium, i.e. equal temperatures, exists between these gases and the solid material. Under these assumptions, three governing equations need to be solved simultaneously.

First, the one-dimensional heat transfer equation considering the pyrolysis behaviour in x-direction is given by:

$$\frac{\partial}{\partial t}(\rho h) = \frac{\partial}{\partial x}(k\frac{\partial T}{\partial x}) - \frac{\partial}{\partial x}(\dot{n}_g h_g) - Q\frac{\partial \rho}{\partial t}$$
(1)

In Eq. (1),  $\rho$  is the instantaneous density of the solid material, so either charred or unpyrolysed material [kg/m³], t is the time [s], T is the temperature [K], x is the location [m], t is the thermal conductivity of the solid material in t direction [W/mK], t and t are enthalpies of the solid material and gas [J/kg], respectively, t is the mass flux of the gas as a product of the pyrolysis [kg/m² s], and t is the so-called heat of decomposition [J/kg]. For this equation, it has been assumed that t runs positively from left to right, and the heat source is to the left of t in the left of the equation is the rate of change of the enthalpy, neglecting the pressure part, so only considering the internal energy part, per unit volume. The first term on the right represents the standard energy contribution thanks to conduction in the solid material, and the second term presents the enthalpy of the escaping gas, which is no longer available to the material [29]. Note that the positive direction for the gas flow is defined from left to right, whereas these gases occur in the pyrolysing material and escape via the char on the left [28]. If the consequently negative valued gas mass flux increases to the left, so the negative values decrease to the left, its derivative to t is positive, and so this leads to a lower enthalpy of the material. The third term relates to the energy that is needed or produced by the pyrolysis. Knowing that for pyrolysis the material density will always decrease, if t has a negative value, the material enthalpy will decrease and so an endothermic reaction takes place. Similarly, a positive value for t indicates an exothermic reaction.

Secondly, the decomposition of the pyrolysing material is given by the Arrhenius Eq. (2) [30]. For an *n*th order reaction:

$$\frac{\partial m}{\partial t} = -A(m_v - m_c) \left[ \frac{m - m_c}{m_v - m_c} \right]^n e^{-\frac{E}{RT}} \tag{2}$$

where m,  $m_v$ , and  $m_c$  are the instantaneous mass, the fully unpyrolysed material's mass, and the fully pyrolysed char's mass [kg], respectively. Symbol A is a so-called "pre-exponential" factor [s<sup>-1</sup>], symbol n the order of reaction, E is the activation energy [J/mol], and E is the universal gas constant 8.314 [J/(mol K)].

Thirdly, if the accumulation of gases is ignored, the mass flux of the pyrolysed gas at an arbitrary location x can be expressed following the conservation of mass as:

$$\dot{m}_{g} = -\int_{L}^{x} \frac{\partial \rho}{\partial t} dx \tag{3}$$

Note that the related equation (4) in [16] is incorrect. First, in their derivation, correctly a minus sign is introduced from [16] equation (3) to [16] equation (4), yielding a plus, because the direction of integration changes from moving right to moving left. But then an additional minus sign should have been introduced, because a value of a function on the left is calculated as a value on the right plus the integration of the differentials. Expanding the left part of the heat transfer Eq. (1) by the chain rule, and defining the specific heat of the solid and gas by  $C_s$  and  $C_g$  yields:

$$\frac{\partial}{\partial t}(\rho h) = \frac{\partial \rho}{\partial t}h + \frac{\partial h}{\partial t}\rho \tag{4}$$

$$C_s = \frac{\partial h}{\partial T}, C_g = \frac{\partial h_g}{\partial T} \tag{5}$$

Two-way coupled fire-structure simulations for real-world structures are 3D, given their realistic nature. For concurrent FEM implementations, it is then convenient, even natural, to define the thermodynamical and thermomechanical equations in 3D too. Including pyrolysis would require coupled integrations in all three Cartesian directions, defined by user subroutines, which is complex implementation-wise. However, for sandwich panels, and probably most other applications of insulation layers, these coupled integrations may not be needed. Namely, the temperature variations over the fire-exposed sandwich panel face are small and the length scale of its surface is large compared to the panel's thickness, so temperature over length gradients are very small. Over the thickness, temperature variations are large, fire-exposed side vs. ambient side, and the length scale is small compared to the panel's surface, so temperature over length gradients are very large. This significant difference in size between gradients over the surface and gradients over the thickness allows for a 1D implementation of pyrolysis, as being driven by these gradients decomposition and mass flux will hardly be a function over the surface but significant over the thickness. Note that in this approach

the temperature distribution is still fully 3D and so is the pyrolysis, for which decomposition and mass flux are solved in the thickness direction, at high resolution over the surface, namely observing each single column of elements over the thickness. What is left out by this approach, only, is the lateral coupling of the pyrolysis decomposition and mass flux in the two directions along the surface, justified by the character of the gradients, whereas the driving conditions themselves, the gradients, are taken into account in 3D. So explicitly, pyrolysis does not depend on temperature variations in y- and z-directions, however, implicitly it does, as these variations, both at the location of interest and in surrounding areas, influence the variations in the x-direction. Consequently, results will always show a 3D distribution of the degree of pyrolysis. Substituting Eqs. (3), (4), and (5) in Eq. (1), and expanding the conduction term into three dimensions, pyrolysis variables remain a function of x only, and a final form of the heat transfer equation is:

$$\rho C_s \frac{\partial T}{\partial t} - \nabla (k_1 \frac{\partial T}{\partial x} \mathbf{i} + k_2 \frac{\partial T}{\partial y} \mathbf{j} + k_3 \frac{\partial T}{\partial z} \mathbf{k}) - C_g \frac{\partial T}{\partial x} \int_{t}^{x} \frac{\partial \rho}{\partial t} dx + \frac{\partial \rho}{\partial t} (Q + h - h_g) = 0$$
(6)

with i, j, k being unit vectors in the x, y, z-direction respectively.

Beyond the above and simplified approach, note that very advanced developments have taken place that allows for full 3D modelling of pyrolysis [31,32], which is relevant for true 3D cases (different from insulation layers) e.g large-scale structure loss [33] and combustible solids [34]. Also, dependent on the type of pyrolysing material, other physical phenomena may need to be modelled. For instance, for polymer composites it is relevant to observe thermal expansion, internal pressure build-up due to the formation of gases, formation of gas-filled pores, matrix cracking, and melting and fusion of fibres [35]. Here, to study the effect of pyrolysis on the temperature distribution on the global scale structure, thermal expansion is believed to be of limited effect as it is zero on average (see Fig. 6 in [35]) and full-scale experiments showed notable expansion only in certain zones [36]. Internal pressure build-up due to the formation of gases can partly be studied by removing the gas flow integral term in Eq. (10), which then shows the behaviour of the simulation is in between models with and without pyrolysis. This is because the pyrolysis still dissipates energy, but the energy normally removed by the outflowing gas is now available to the system. The formation of gas-filled pores, and their behaviour under high gas pressures is a very complex subject, still under investigation [35]. However, as will be shown in Section 3.2, the omission of modelling this aspect does not seem to influence the accurate description of the temperature distribution in time due to pyrolysis, which is the focus of this paper. Finally, matrix cracking and melting and fusion of fibres are not relevant to the PIR material studied in this paper.

#### 2.2. Finite element implementation

In a finite element analysis, heat transfer can be defined as [37]:

$$\int_{V} \rho \dot{U} dV = -\int_{V} \frac{\partial}{\partial \mathbf{x}} \cdot \mathbf{f} dV + \int_{V} r dV, \text{ with } \mathbf{x} = [x \ y \ z]$$
(7)

$$\mathbf{f} = -k_1 \frac{\partial \mathbf{T}}{\partial x} \mathbf{i} - k_2 \frac{\partial \mathbf{T}}{\partial y} \mathbf{j} - k_3 \frac{\partial \mathbf{T}}{\partial z} \mathbf{k}$$
 (8)

where V is the volume of solid material,  $\dot{U}$  is the rate of the internal energy,  $\mathbf{f}$  is the heat flux vector, and r is the heat supplied externally into the body per unit of volume.

The following variables must be predicted at the end of a time increment: the internal energy U, also given at the start of the increment, its derivative with respect to temperature  $\partial U/\partial T$  and to spatial gradients of temperature  $\partial U/\partial (\partial T/\partial x)$ , the heat flux vector  $\mathbf{f}$ , and its derivatives with respect to temperature  $\partial \mathbf{f}/\partial T$  and spatial gradients of temperature  $\partial \mathbf{f}/\partial (\partial T/\partial x)$ . Including pyrolysis, the variables to be predicted can be obtained as follows. If the energy balance in Eq. (7) is interpreted for infinitesimal volume, so integrals vanish, it includes the internal energy, contributions of conduction, and heat supplied externally. If pyrolysis (Eq. (6)) is included in the finite element analysis (Eq. (7)), the internal energy rate in Eq. (7) should contain:

$$\dot{U} = \rho C_s \frac{\partial T}{\partial t} - C_g \frac{\partial T}{\partial x} \int_t^x \frac{\partial \rho}{\partial t} dx + \frac{\partial \rho}{\partial t} (Q + h - h_g)$$
(9)

where l is the length of the specimen, which is, based on the assumptions in Section 2.1, numerically equal to the position at the complete right. Using a finite difference approximation, the incremental form of Eq. (9) can be written as:

$$\Delta U = \rho C_s \Delta T - C_g \frac{\partial T}{\partial x} \int_l^x \Delta \rho dx + \Delta \rho (Q + h - h_g)$$
(10)

Using Eq. (10), the internal energy at the end of time increment  $U(t + \Delta t)$  can be predicted by the energy at the beginning of the time increment U(t), the latter given by the analysis:

$$U(t + \Delta t) = U(t) + \Delta U \tag{11}$$

For the prediction of the derivatives mentioned above, the internal energy is a function of time, temperature, and density, the latter two themselves functions of position. Therefore, the total derivative of the internal energy with respect to time is [18]:

$$\frac{dU}{dt} = \frac{\partial U}{\partial t} + \frac{\partial U}{\partial T}\frac{dT}{dt} + \frac{\partial U}{\partial (\partial T/\partial \mathbf{x})} \cdot \frac{d(\frac{\partial T}{\partial \mathbf{x}})}{dt} + \frac{\partial U}{\partial \rho}\frac{d\rho}{dt} + \frac{\partial U}{\partial (\partial \rho/\partial \mathbf{x})} \cdot \frac{d(\frac{\partial \rho}{\partial \mathbf{x}})}{dt}$$
(12)

Comparing Eqs. (12) and (9) yields:

$$\frac{\partial U}{\partial T} = \rho C_s \tag{13}$$

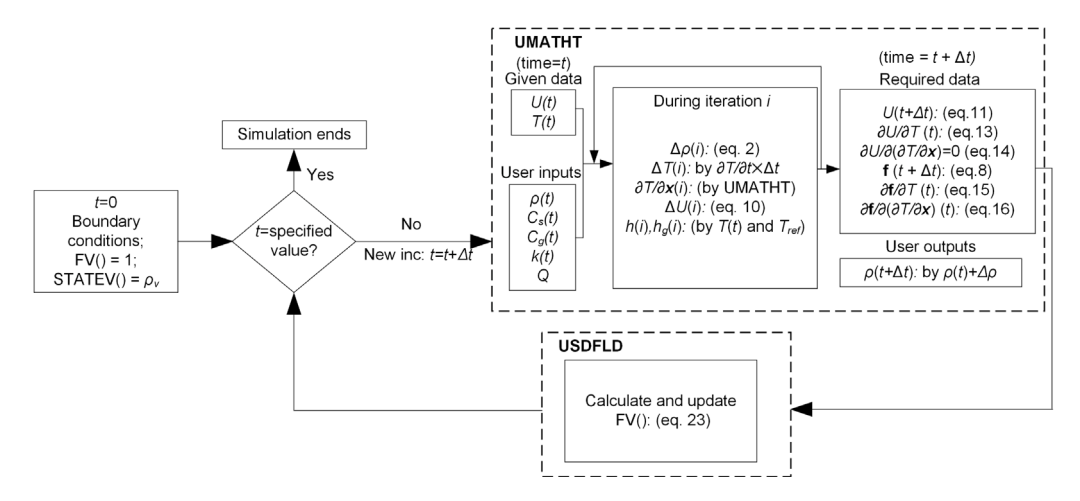


Fig. 1. Implementation of the pyrolysis model via the Abaqus UMATHT and USDFLD user subroutines.

$$\frac{\partial U}{\partial (\partial T/\partial \mathbf{x})} = \mathbf{0} \tag{14}$$

For the heat flux in Eq. (8), the derivative with respect to the temperature and the temperature gradients can be written as:

$$\frac{\partial \mathbf{f}}{\partial T} = -\frac{\partial T}{\partial x} \frac{\partial k_1}{\partial T} \mathbf{i} - \frac{\partial T}{\partial y} \frac{\partial k_2}{\partial T} \mathbf{j} - \frac{\partial T}{\partial z} \frac{\partial k_3}{\partial T} \mathbf{k}$$
(15)

$$\frac{\partial \mathbf{f}}{\partial (\partial T/\partial \mathbf{x})} = \begin{bmatrix} -k_1 & 0 & 0\\ 0 & -k_2 & 0\\ 0 & 0 & -k_3 \end{bmatrix}$$
 (16)

Fig. 1 presents a flowchart of this finite element implementation in Abaqus, with so-called subroutines UMATHT and USDFLD. At the start of the HT analysis, t = 0, the FEM should be given thermal boundary conditions: heat flux, temperatures, radiation, etc. The Field Variable FV() indicates the level of pyrolysis, is initialised as 1, and indicates fully pyrolysed material when equal to 0. State variable STATEV() is a variable in Abaqus that indicates the instantaneous density of each integration point, and the initial value should equal the value of the virgin material density. While not at the end of the simulation, a time increment  $\Delta t$  is taken, and for each iteration within the increment, the user subroutine UMATHT is predicting the variables as shown in Fig. 1. The kinetic parameters (reaction order, activation energy, and pre-exponential factor) as used in Eq. (2) are used for the calculation of  $\Delta \rho(i)$ . Note that the determination of these parameters is subject to research [38], and that the values used in this research are listed during the presentation of the simulations. Finally, it should be mentioned that some variables at the end of the increment are calculated for t, which is comparable to a modified Newton–Raphson procedure. User subroutine USDFLD is used to keep track of the FV() of each integration point, over all time increments and iterations.

The second term on the right of Eq. (10) shows the integration of the gas mass in negative x-direction. This integration needs to take place on the model level, rather than on the element level, which is carried out as shown in Fig. 2. On the left, for a 2D case using 4-node quadrilateral shell elements, DS4 in Abaqus, for each iteration the pyrolysis increase  $\Delta \rho$  for each integration point, indicated by a cross, is obtained by Eq. (2), as explained above. This increase is subsequently multiplied by the point's representative length in x-direction, in this case half the element height, and contributions of all relevant integration points, coloured red in the figure, are summed up for the integral. For a 3D case as shown on the right, using 8-node linear heat transfer brick elements, DC3D8 in Abaqus, the same procedure is followed: also here the pyrolysis increase is multiplied with the representative length in x-direction, so not by the area or volume.

# 2.3. Coupled fire-structure simulations

For a coupled fire-structure simulation, first the fire is simulated in the Computational Fluid Dynamics (CFD) domain. Here, the Fire Dynamics Simulator (FDS) has been used, which applies large eddy simulations, ignoring the smallest length scales of the Navier–Stokes equations, verified to be appropriate for smoke and heat phenomena in fires [39,40]. The thermal data of the fire simulation is used for an HT analysis, which subsequently provides temperatures for an SR analysis, both in the FEM domain, see Fig. 3. In this figure, couplings (A1) and (A2) have been mentioned earlier, and without (A3), the resulting simulations are defined as OWC. If additional structural changes, e.g. a panel falling off, are included in the following fire simulations, indicated by (A3), a TWC simulation is carried out [41,42]. Naturally, the accuracy of such a TWC simulation is dependent on the load step sizes used. Implementation details are given in Section 4 and in [41,42], whereas here the general concept of the transfer of thermal data from

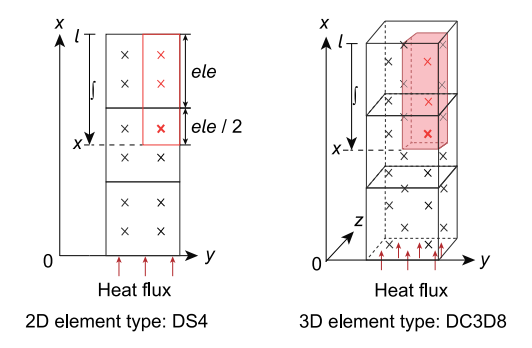


Fig. 2. Integration of gas mass on the model level, "ele" is the element height. (For interpretation of the references to colour in this figure legend, the reader is referred to the web version of this article.)

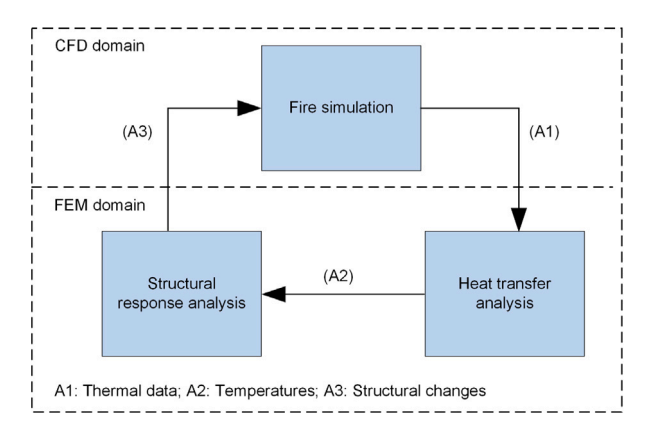


Fig. 3. Coupled fire-structure simulations: TWC if A3 is present.

the fire simulation to the HT analysis via the AST [27] is explained. During a fire, energy is transferred from the flames to the surrounding structural surfaces via radiation and convection. The related heat flux  $q_{total}$  can be expressed as:

$$q_{total} = q_{rad} + q_{cv} \tag{17}$$

where the convective flux  $q_{cv}$  [W/m<sup>2</sup>] depends on the difference between the gas temperature  $T_g$  and the structural surface temperature  $T_{surf}$  [K], and the convective heat transfer coefficient  $h_{cv}$  [J/(kg K)]:

$$q_{cv} = h_{cv} (T_g - T_{surf}) \tag{18}$$

The radiant flux  $q_{rad}$  [W/m<sup>2</sup>] is given by:

$$q_{rad} = \varepsilon \sigma (T_{amb}^4 - T_{surf}^4) \tag{19}$$

where  $\varepsilon$  is the emissivity of the surface,  $\sigma$  is the Stefan Boltzmann constant  $5.6703 \times 10^{-8}$  [W/(m² K⁴)], and  $T_{amb}$  and  $T_{surf}$  are the absolute ambient and surface temperature [K], respectively. The AST is defined as the temperature of an imaginary perfect insulator, exposed to the same fire conditions as the real surface. For such an imaginary insulator, the total flux  $q_{total}$  is zero, and the AST can be calculated by setting  $q_{total}$  to zero, and substituting the AST for  $T_g$  and  $T_{amb}$  in Eqs. (17) to (19). Then in a FEM, the flux on the structure can be calculated:

$$q_{total,fem} = \varepsilon \sigma (AST^4 - T_{surf,fem}^4) + h_{cv}(AST - T_{surf,fem})$$
(20)

where  $T_{surf,fem}$  is the surface temperature in the model. By using the AST, the dependency of the surface temperature on the heat flux is eliminated. A similar method is adopted by others, e.g. [43].

#### 3. Verification and validation of the pyrolysis model

Coupled fire-structure simulations have been verified before [41,42]. However, the implementation of the pyrolysis model, as will be used here within these fire-structure simulations, has not yet been verified. Therefore the pyrolysis model will be verified by (a) a pyrolysis model by Zhang [18], and (b) validated by an experiment by Henderson [16]. Note that the pyrolysis model by Zhang follows the equations in Section 2.1, and so is equivalent to the model in this paper. However, Zhang's implementation in the

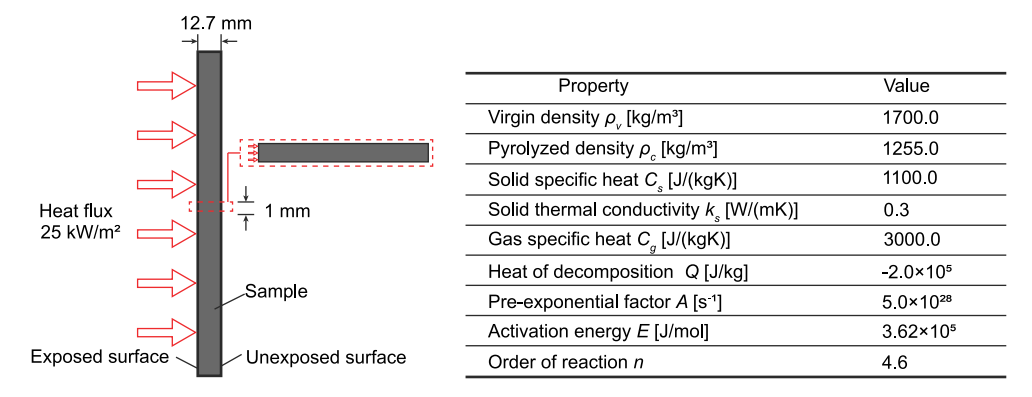


Fig. 4. Test case, geometry and properties.

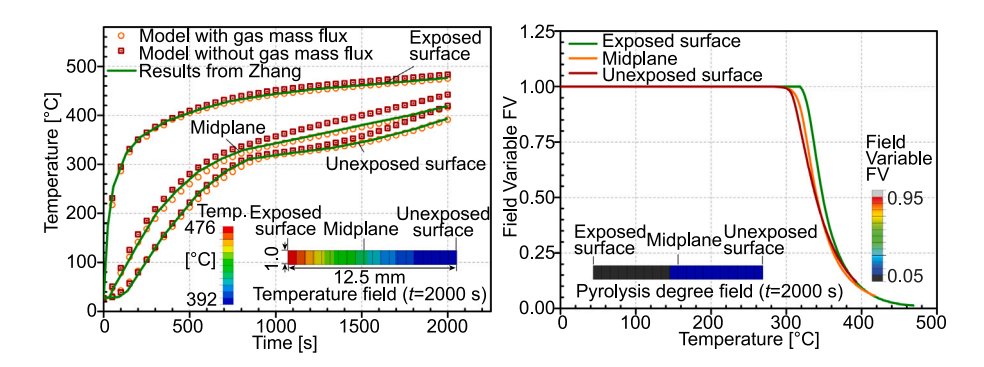


Fig. 5. Verification of the pyrolysis model. (For interpretation of the references to colour in this figure legend, the reader is referred to the web version of this article.)

finite element method, on the code level, is not available open-source, so is likely to be different. For this paper, code and scripts to reproduce all the simulations are available on GitHub [26]. The experiment by Henderson has such a set-up that all elements of the pyrolysis model can be validated. For significantly different materials, e.g. the composites mentioned before [35], further validation with a broader array of experimental data is recommended.

#### 3.1. Verification by existing model

A 2D test case [18] is shown in Fig. 4. Natural (Neumann) boundary conditions involve the left surface of the sample being loaded uniformly by a heat flux equal to  $25 \text{ kW/m}^2$ . For the other surfaces no explicit conditions are given, so the flux equals zero there. Essential (Dirichlet) boundary conditions are not needed as a transient simulation is carried out for a limited period. Initial temperatures are  $27 \,^{\circ}$ C. To avoid any 2D effects, only a slice of a height of 1 mm is modelled, with properties as shown in the figure on the right. The top, bottom, and left sides are unconstrained, in practice meaning fluxes there must be zero. Two simulations are carried out by a transient HT analysis, see Sections 2.2 and 2.3, using 2D and 3D elements respectively, the latter to ensure their proper application later on. For 2D, DS4 elements  $1 \times 0.625 \, \text{mm}^2$  in size are used, and for 3D, volume elements DC3D8  $1 \times 1 \times 0.625 \, \text{mm}^3$  in size are applied. A fixed time increment of 50 s is used in the analysis. For the 2D case, at time  $t = 2000 \, \text{s}$ , Fig. 5 on the left shows temperatures versus time for the existing results from Zhang [18] by green lines, and the implemented pyrolysis model by the orange markers. The two models predict the same behaviour for all three surfaces, exposed surface, midplane, and unexposed surface, despite slightly different implementations. Fig. 5 on the right shows, for the same model and time, along all elements, the temperature vs. the field variable FV, which indicates the pyrolysis level, from 0 to 1, with 0 for fully pyrolysed. It can be seen that the implemented model performs as expected, as lower temperatures do not show pyrolysis, and increasingly higher temperatures do. Additionally, the results show that most loss of mass (90%) occurs in a window between 300 and 420 °C. For the 3D case, the results are exactly the same, and so are not shown here.

In the pyrolysis model, it is assumed that the generated gas can flow out via the charred material, i.e. accumulation of gases will not occur. Consequently, the heat energy contained in the gas will not be available to the problem. However, this assumption may not be valid in practice, for instance, for a sandwich panel where the pyrolysing material is enclosed by airtight plates. To study the related effects, an additional simulation has been conducted, in which the second term on the right in Eq. (10) is neglected. The results are shown in Fig. 5 on the left with red square markers, which show a small increase in temperatures, as expected. Note,

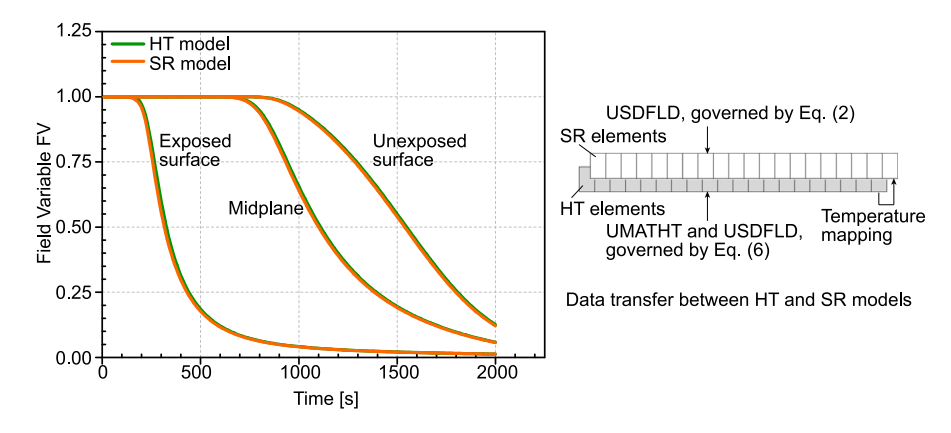


Fig. 6. Verification of the FV transfer between the HT and SR models.

however, that the accumulation of gases and related increasing pressures may affect the pyrolysis process, which is not taken into account in the equations.

Finally, the case is also used to check the implementation for the calculation of the pyrolysis level in the SR model. Namely, the Field Variable FV indicating the pyrolysis level cannot be transferred directly from an HT to an SR model. It is, however, needed for the SR-dependent material properties. As a workaround, the implementation transfers the temperature vs. time data from HT to SR, and then the pyrolysis level is recalculated in the SR by an Abaqus USDFLD user subroutine, using Eq. (2). The results are shown in Fig. 6, which shows on the left the Field Variable FV vs. time for several surfaces, for which the SR gives the same values as the HT model. On the right, the meshes of the HT and SR models are shown schematically. The FV in the SR analysis is calculated by the UMATHT and USDFLD subroutines, as explained in Section 2.2. The resulting pyrolysis levels influence the temperature distribution in time. As mentioned, this temperature distribution is given to the SR analysis, which uses a USDFLD subroutine to recover the corresponding FV. Note that for the specific finite element programme used, structural elements with the same order as the HT thermal elements DS4 and DC3D8, see e.g. Fig. 2, only provided a constant temperature over the element, although the HT model provides linearly varying temperatures, and for this situation, the graphs in Fig. 6 are not corresponding. By using higher-order elements for the SR analysis, i.e. S8R and C3D20R, this problem is solved, and so these elements are also used in the upcoming simulations.

#### 3.2. Validation by existing experiment

Henderson et al. reported on an experiment with phenolic resin, exposed to a heat flux on one side, to research the pyrolysis of this material [16]. Similar to the case in the previous section, mechanical behaviour was not studied. The phenolic resin was made by 39.5% resin and 60.5% filler, machined to a 30 mm long cylinder, with a 10 mm diameter. The bottom end of the vertically positioned cylinder was exposed to a radiant heat flux of 279.7 kW/m $^2$  for 800 s. Temperatures were measured inside the sample, at depths of y = 1, 20, 25, and 29 mm.

To simulate this experiment, a transient HT analysis is carried out as explained in Sections 2.2 and 2.3, and shown in Fig. 7. The elements used are "DC3D8", on average  $1 \times 1 \times 1$  mm<sup>3</sup> in size. The material properties used are shown in Table 1, for which the parameters related to the pyrolysis (A, n, E) were obtained from thermogravimetric analysis [16]. The specific heat of the virgin and pyrolysed material are temperature-dependent, and these properties were measured by differential scanning calorimetry [44]. The thermal conductivity of these materials is also temperature-dependent, for which data was obtained by experiments reported elsewhere [45]. The thermal properties in the table only apply to materials that are either completely virgin or pyrolysed. Linear interpolation is applied for the thermal conductivity k and specific heat C of partly pyrolysed material:

$$k = Fk_{r} + (1 - F)k_{r} \tag{21}$$

$$C = FC_v + (1 - F)C_c (22)$$

where F is defined as the ratio of the current mass of virgin material over the total potential mass lost due to full pyrolysis:

$$F = \frac{m - m_c}{m_v - m_c} \tag{23}$$

Natural (Neumann) boundary conditions involve the right surface of the sample being loaded uniformly by a heat flux equal to 279.7 kW/m<sup>2</sup>. For the other surfaces no explicit conditions are given, so the flux equals zero there. Essential (Dirichlet) boundary conditions are not needed as a transient simulation is carried out for a limited period. Fig. 8 shows that the implementation of the pyrolysis model into the HT model predicts the experimental measurements reasonably well. Some differences exist, though,

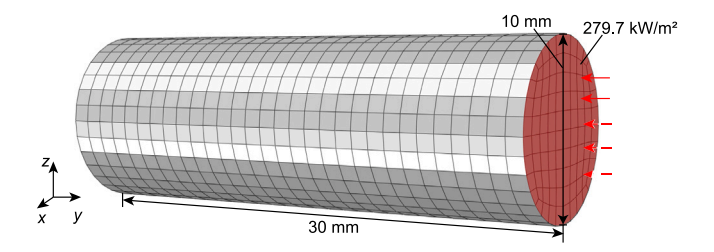


Fig. 7. HT analysis model for experiment Henderson et al. [16].

Table 1 Material properties used for validation.

Property	Value
Virgin material density $\rho_v$ [kg/m <sup>3</sup> ]	1810
Pyrolysed material density $\rho_c$ [kg/m <sup>3</sup> ]	1440
Virgin material specific heat C <sub>n</sub> [J/(kg K)]	1890 + 1.09T
Virgin material thermal conductivity $k_n$ [W/(mK)]	$0.804 + 2.76 \times 10^{-4}T$
Pyrolysed material specific heat C <sub>c</sub> [J/(kg K)]	870 + 1.02T
Pyrolysed material thermal conductivity $k_c$ [W/(mK)]	$0.955 + 8.42 \times 10^{-4}T$
Gas specific heat $C_g$ [J/(kg K)]	9630
Heat of decomposition $Q$ [J/kg]	$2.34 \times 10^{5}$
Activation energy $E$ [J/mol]	$2.60 \times 10^{5}$
Pre-exponential factor $A[s^{-1}]$	$8.16 \times 10^{18}$
Order of reaction n	6.3

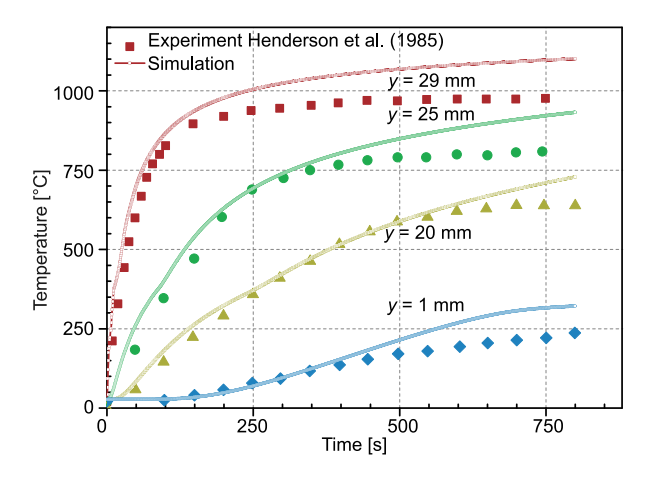


Fig. 8. Experiment Henderson et al. (curves) vs. HT model + pyrolysis (markers).

likely because not all physical phenomena are modelled, e.g. the non-steady diffusion of decomposition gases, thermal expansion, carbon–silica reactions, and the heat transfer between the gas and pyrolysed material.

The simulation is also beneficial for understanding some behaviour of pyrolysis that an experiment cannot easily reveal: Fig. 9 on the left shows the pyrolysis reaction rate vs. time, in the simulation, for different locations in length direction. The contour plots on the right show the degree of pyrolysis, i.e. the Field Variable FV at several times t: 200, 400, 600, and 800 s, respectively. It can be seen that the active, coloured, region, where pyrolysis takes place, increases in size over time. This is because each slice of material needs an equal amount of energy (the integral of the curves on the left) to fully pyrolyse, whereas the flux entering from the right is dissipated by the pyrolysis reaction and material heat capacity. This leads to increasingly equalised and stretched temperature profiles when moving further away from the heat source.

#### 4. Fire-structure simulations, software and scripts

In the previous sections, the pyrolysis implementation has been verified and validated, and also the concept of OWC and TWC fire-structure simulations has been explained. In this section, the setup of the fire-structure simulations is further elaborated, including an explanation of the software used and programmes and scripts developed. This then enables the presentation of the case study in Section 5, which applies the fire-structure simulations to study the effects of the inclusion of pyrolysis.

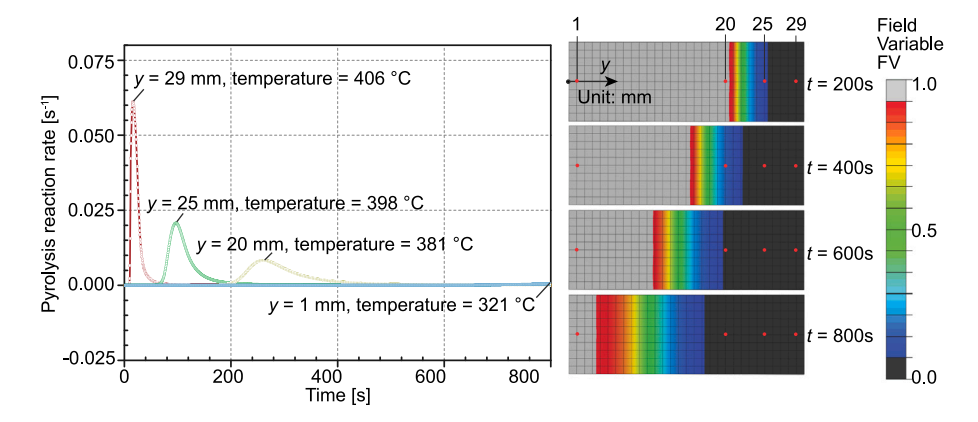


Fig. 9. Pyrolysis reaction rate at different locations along the length. (For interpretation of the references to colour in this figure legend, the reader is referred to the web version of this article.)

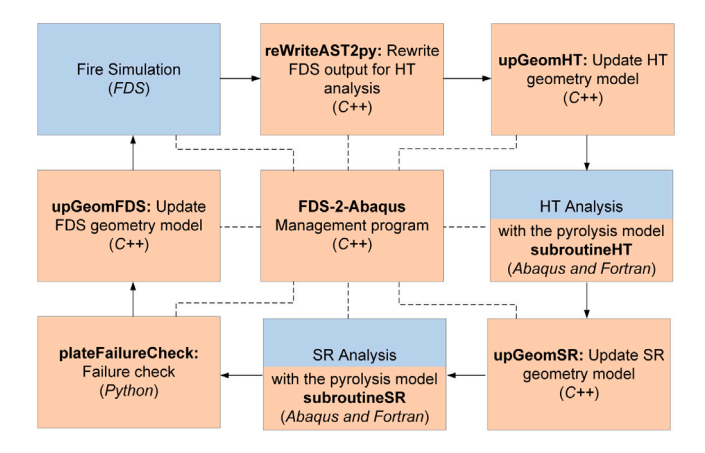


Fig. 10. Implementation of the pyrolysis model in TWC fire-structure simulations, one cycle equals one load step. (For interpretation of the references to colour in this figure legend, the reader is referred to the web version of this article.)

The implementation of the fire-structure simulations is based on the work of Feenstra et al. [41] and De Boer et al. [42]. Based on their developments, Fig. 10 presents the software and scripts used in this paper, in the outer ring, where blue boxes refer to public or commercial software, and orange boxes to in-house developed programmes or scripts. In the middle, "FDS-2-Abaqus" is a management programme, which e.g. starts and stops the programmes and scripts, and controls overall variables like the load step size. Each fire-structure simulation starts with a fire simulation by FDS [39], shown at the complete left upper corner in Fig. 10. Then the HT and SR analyses are carried out, both by finite element programme Abaqus [37]. In between, several C++ programmes and Python scripts are used, as explained further below. All programmes and scripts, for all simulations in this paper, are published open-source on GitHub, to enable further developments and full reproducibility of the findings.

#### 4.1. reWriteAST2py

Following [41,42], the fire simulation pauses at the end of each load step, whereafter this C++ programme writes the AST data into a Python script that can be read by Abaqus, see also Section 2.3.

#### 4.2. upGeomHT

The programme upGeomHT generates, or updates for subsequent load steps, the script that is needed to run the HT analysis, including the calls to the pyrolysis user subroutines in Abaqus. The generated script contains geometrical information, such as parts and partitions, material properties, the mesh, assemblies, interactions, etc. During two-way simulations, the script may also contain (a) failure information of structural elements and (b) the updated time–temperature data as provided by reWriteAST2py. Namely, for two-way simulations any failed element is deactivated by a proprietary Abaqus "model change interaction", and such an element will not be taken into account in subsequent analyses.

#### 4.3. subroutineHT and subroutineSR

These two Fortran user subroutines are used to predict the pyrolysis behaviour of the insulation material, and are incorporated within the HT and the SR analyses. SubroutineHT predicts the pyrolysis behaviour via the user subroutines UMATHT and USDFLD, as explained in Fig. 1. In subroutineSR, only the degree of pyrolysis is calculated, by using Eq. (2) within the user subroutine USDFLD.

#### 4.4. upGeomSR

Similar to upGeomHT, the programme upGeomSR generates or updates the input file for the SR analysis. This input file includes the required calls to the subroutineSR, and the importing of nodal temperatures from the previous HT analysis. Deactivation of failed elements is analogous to the procedure as explained in Section 4.2.

#### 4.5. PlateFailureCheck

At the end of each load step, the Python script plateFailureCheck checks the failure status of each structural element. The script extracts information from the SR model, including displacement values of nodes related to panels, bolts, and screws. Based on various Eurocodes [46–48], this information is used to assess structural failure, and consequently the corresponding element may be removed from subsequent load steps.

#### 4.6. upGeomFDS

Similar to upGeomHT and upGeomSR, the programme upGeomFDS updates the scripts needed to run FDS. The programme copies the basic setup, e.g. the fire compartment geometry, and modifies it by removing the failed structural elements. Further details, including code and scripts of the fire-structure analysis, but without pyrolysis, can be found in Refs. [41,42].

#### 5. Case study

In Section 5, the pyrolysis implementation of Section 2 is used in combination with fire-structure simulations to model a case study. The case study aims to demonstrate that the effects of pyrolysis on the temperature distribution, and temperature and pyrolysis-dependent mechanical material properties, can be taken into account in fire-structure simulations on the global scale. This is with a pyrolysis model that is computationally efficient and easy to implement, yet reasonably accurate, thanks to the large differences in temperature gradients over the surface versus depth for insulation layers.

The case involves an office room with a sandwich panel facade. The facade consists of three panels, each having two steel faces and a PIR insulation core, and all fixed to steel columns by connections. The case study is taken from a paper by De Boer et al. [42], and additionally uses the pyrolysis model for the PIR insulation cores. The modelling of the mechanical response precisely follows De Boer et al. [42], for verification purposes, and within that framework, the pyrolysis model influences the temperature distribution and the temperature and pyrolysis-dependent properties, as further described below. Experimental validations of sandwich panels under fire on the global scale have been carried out [49], but not including pyrolysis effects. For the latter, dedicated experiments need to be designed in the future.

First, an overview of the model setup is given in Section 5.1, including a description of the fire simulation and the finite element model. In Section 5.2, the effect of pyrolysis is studied for the case study, in which panels fall off within 100 s due to their screw connections failing by shear. To study pyrolysis for a longer period, Section 5.3 prolongs the case study to 1800 s, neglecting connection failures.

# 5.1. Model setup

The simulations start with a fire simulation by FDS, modelling a compartment,  $5.4 \times 3.6 \times 2.7 \text{ m}^3$  in size, see Fig. 11, and using cubic CFD elements  $0.15 \times 0.15 \times 0.15 \text{ m}^3$  in size. On the sides of the compartment, two additional spaces are modelled, for a corridor and outside space respectively, to allow for airflow into the compartment. Between the corridor and compartment, a door with a width of 0.9 m and a height of 2.1 m is modelled for this purpose. A one-hour fire is simulated, with cellulose selected as a fuel, having a specified Heat Release Rate Per Unit Area (HRRPUA) of  $250 \text{ kW/m}^2$ , as suggested by Eurocode 1993-1–2 [50]. The walls, floors (except the facade) and ceiling of the office room are assumed to be concrete, in FDS being "obstructions" with a thickness of 0.3 m, density of 1800 [kg/m³], specific heat of 1.00 [kJ/(kg K)], conductivity of 1.15 [W/(mK)], and emissivity of 0.8. The facade consists of 3 sandwich panels with adiabatic properties, each having 16 AST data points to record the AST, as explained in Section 2.3.

The finite element model simulates the facade system, which consists of three 3.6 m  $\times$  0.9 m sandwich panels, each having an outer steel face, thickness of 0.5 mm, an inner steel face, thickness of 0.4 mm, and an 80 mm thick PIR insulation core, see Fig. 12. Each panel is fixed at its bottom via a tongue-and-groove joint with the panel below, and at its left and right upper corner to a vertical cold-formed L-section by a screw. The L-sections are connected by bolts to lips welded to two HE200 A columns.

For thermodynamical simulations, an HT model is used as shown in Fig. 12 on the left. Each sandwich panel is divided into 16 partitions, where each partition's inner face will inherit the AST value of the corresponding AST point in the fire simulation.

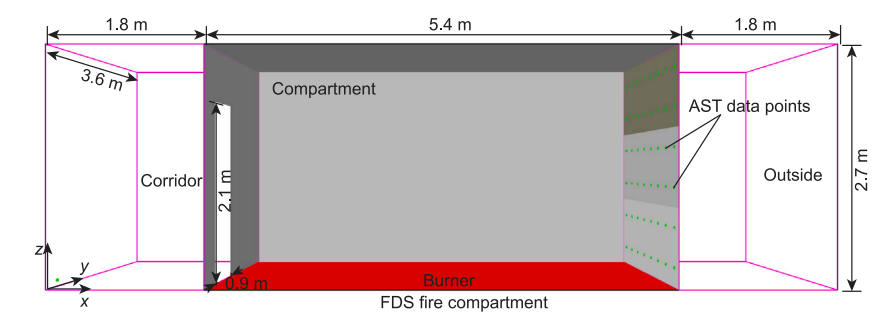


Fig. 11. Setup of the fire compartment in FDS.

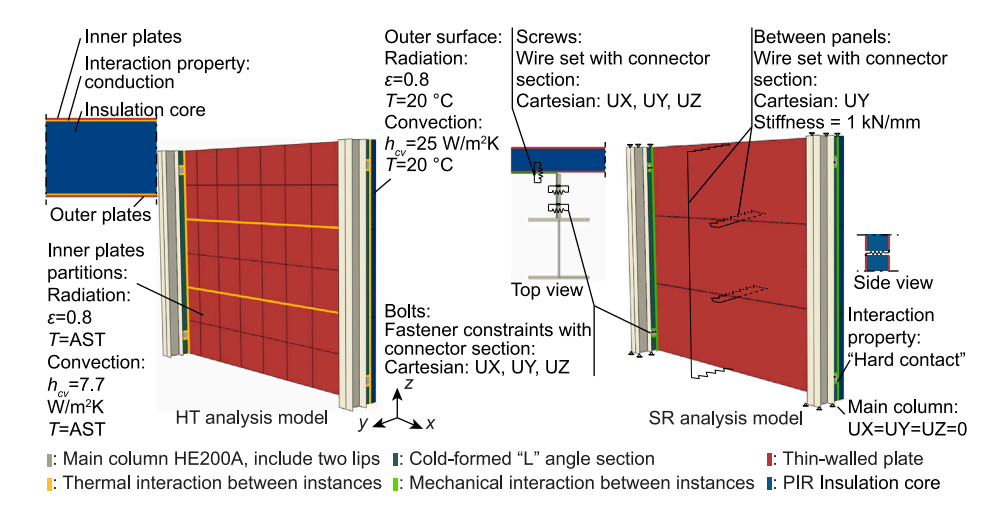


Fig. 12. Setup of finite element models for sandwich panel facade.

Table 2
PIR material properties as used in the simulations.

Pik material properties as used in the simulations.	
Property	Value
Virgin material density $\rho_v$ [kg/m <sup>3</sup> ]	80, Ref. [52]
Pyrolysed material density $\rho_c$ [kg/m <sup>3</sup> ]	20.4, Ref. [52] Fig. 1
Solid specific heat $C_s$ [J/(kg K)]	4.86T - 357, Ref. [53] Table 2
Solid thermal conductivity $k_s$ [W/(mK)]	$2 \times 10^{-7} T^2 - 9 \times 10^{-5} T + 0.0397$ , (table 3-2 in [54])
Gas specific heat $C_g$ [J/(kg K)]	2100, Ref. [53]
Heat of decomposition Q [J/kg]	-3.98×10 <sup>5</sup> , Ref. [53] Table 1
Pre-exponential factor $A$ [s <sup>-1</sup> ]	2.344×10 <sup>8</sup> , Ref. [52] Table 8
Activation energy E [J/mol]	1.01×10 <sup>5</sup> , Ref. [52] Table 8
Order of reaction n	4, Ref. [52] Table 8

Regarding the mesh, the columns, L-sections, and the faces of the panels are modelled with  $50 \times 50$  mm DS8 eight-node heat transfer quadrilateral shell elements. The core is developed by DC3CD20 brick elements. For steel, its thermal conductivity and specific heat are taken from EN 1993-1-2 [51] Section 3, see for further details [42]. For simulations without pyrolysis, the PIR core is modelled with a conductivity equal to 0.023 [W/(mK)], and a specific heat of 1400 [J/(kg K)], to enable verification with previous work [42]. If pyrolysis is modelled, the properties of the PIR core are listed in Table 2, including their source. Concerning the conductivity between instances, so-called interaction properties are used, indicated by the bold orange lines. The inner and outer faces of the panels have radiation and convection properties as indicated in the figure. Loading takes place by setting the temperatures of the inner face to the ASTs found by the fire simulation, and setting the outer face temperatures to 20 degrees. A transient solver is used, and further details can be found in [42].

After the determination of the temperature distribution over time, an SR analysis model, shown in Fig. 12 on the right, predicts the structural response. The model follows the setup of the HT model, but for the shell elements mechanical S8R eight-node quadratic shell elements are used, and for the insulation core mechanical C3D20R elements are applied. For steel, grade S355 is used, which has an ambient Young's modulus of  $2.1 \times 10^5$  N/mm<sup>2</sup>, a yield strength of 355 N/mm<sup>2</sup>, and an ultimate strength of 490 N/mm<sup>2</sup>, all as recommended in EN 1993-1-1 [55]. The temperature-dependent values for Young's modulus and strength, including thermal

properties such as thermal conductivity and specific heat are taken from EN 1993-1-2 [51] Section 3. Regarding the PIR insulation core, mechanical properties are mostly taken as constant as listed in De Boer's paper [42], including a Young's modulus of 20000 N/mm<sup>2</sup>, a Poisson ratio of 0.2, and a thermal expansion coefficient of  $5.0 \times 10^{-5}$ . However, for each integration point, Young's modulus is halved when the PIR is fully pyrolysed at that point. The contact between instances is modelled by "hard contact interaction properties", which is indicated by the bold green lines.

The tongue-and-groove connections, bolts, and screws are modelled by linear elastic springs, via Abaqus "Connection Sections" with translational type "Cartesian". Their stiffness values are determined following the "component method" in Eurocode 1993-1-8 [48]. Observed failure modes are related to (a) panel failure, implemented via a check on the maximal panel deflection; (b) facade openings, measured via the difference in nodal displacement above and below the tongue and groove connection; (c) panel-angle section screw failure, checked by Eurocode 1999-1-4 [46] design rules for (i) the combination of shear and tension in the screw, (ii) shear failure of the screw, (iii) bearing failure of the thin-walled angle section, (iv) tension failure of the screw, and (v) pull-out resistance of the screw; and (d) main structure column-angle section bolt failure, predicted by Eurocode EN 1993-1-8 [48] design rules for (i) combination of shear and tension in the bolt, (ii) shear failure of the bolt, (iii) bearing failure of the angle section, (iv) tension failure of the bolt, and (v) punching shear resistance of the angle section.

The SR model is used to investigate the action of the temperature loads, and so no further mechanical loads are applied. To solve the system of equations, a general static solver is used. Further details, especially on the connection stiffness values and failure criteria, can be found in [42], and fully coded in [26].

#### 5.2. Simulations

Simulations use the software and scripts as explained in Section 4 and the model setup as presented in Section 5.1, illustrated in Fig. 13 with a typical simulation including pyrolysis.

First, for verification purposes, a standard TWC simulation (TWC and not OWC, as TWC is the more extended and general approach) of De Boer et al. was run, so without pyrolysis: the "Two-way CFD-FEM coupling" simulation in their (figure 12 [42]). Original code and scripts were used, and results are shown in Fig. 14. For the rerun, the bottom, middle, and top panels fail at 45, 55, and 70 s respectively, all by their two screws failing by shear following displacement-controlled failure checks [42]. However, in the original paper, these numbers were 40, 45, and 60 s. The code and scripts were checked and deemed to be correct for the settings stated in the paper, and so apparently other settings were used to produce (figure 12 in [42]). Code and scripts to reproduce all the simulations in this paper are available [26], and so the results in Fig. 14 will be used for further studies.

Second, the same simulation was carried out, but with pyrolysis included. At the top left of Fig. 13, the fire simulation is shown, including the corridor, compartment, outside region, panels, and AST data points clearly visible for Panel 3. In total, a 100-s fire is simulated, by 10 equal load steps of 10 s. After the first load step, the AST data is transferred to the FEM domain for a first HT analysis, top right. As mentioned earlier, each of the 16 partitions of each panel will be loaded at the inner side by a temperature equal to the AST value of the related AST point in the fire simulation. The HT analysis predicts, via the UMATHT and USDFLD subroutines, see Fig. 1, the pyrolysis level at each integration point (middle row, left) in combination with the temperature distribution. Then, the nodal temperatures vs. time as found in the HT analysis are transferred to the SR analysis (middle row, right) which subsequently predicts displacements, strains, and stresses over the time of the load step. Note that for practical reasons, the SR analysis recalculates the pyrolysis levels of each integration point. After the SR analysis, several failure criteria are checked [42], and a panel is removed if it has failed. Then the fire simulation is restarted, now with the failed panel removed, and this iterative process is followed until the final time step has been finished.

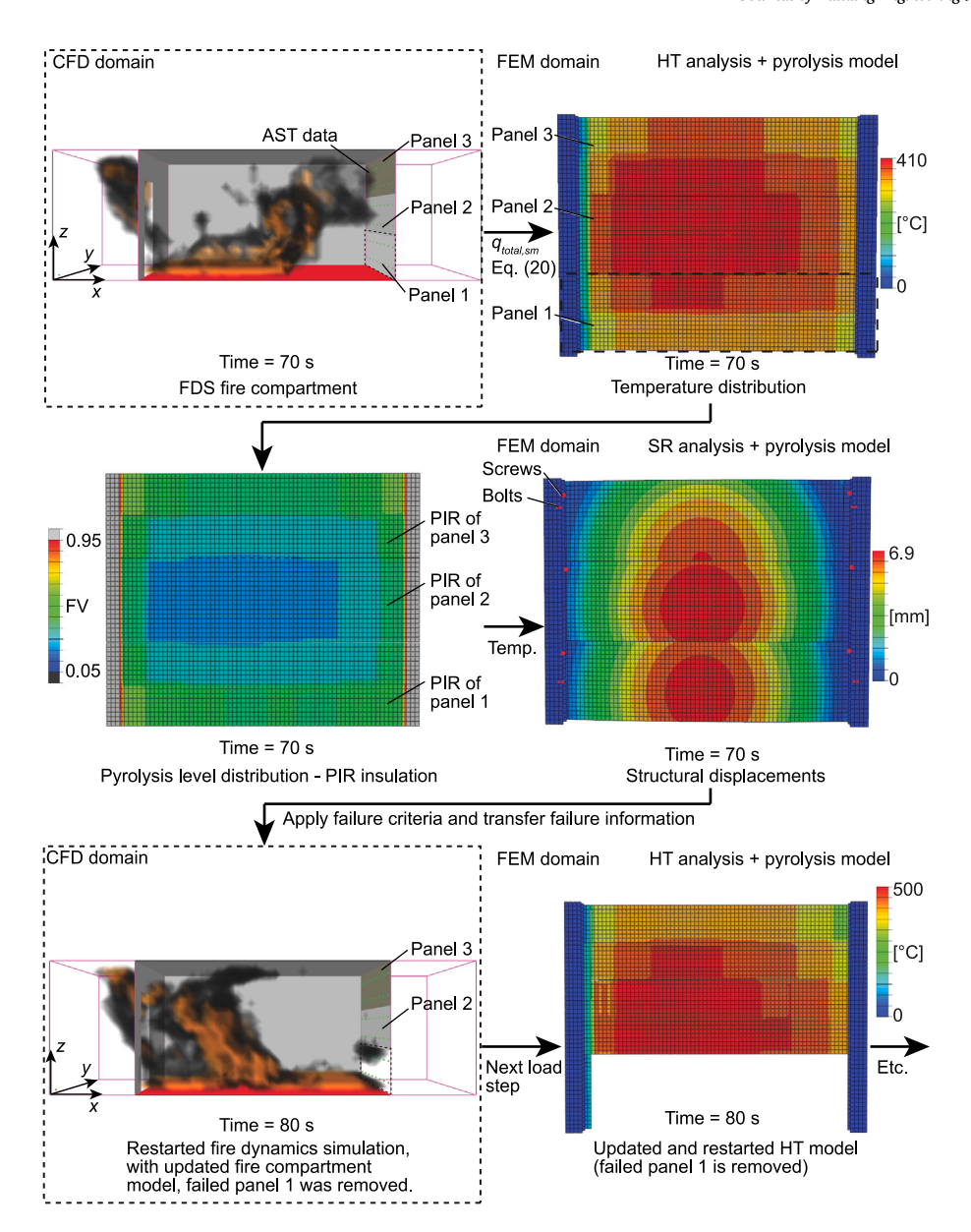
Fig. 14 shows that the inclusion of pyrolysis delays the failure of the panels, which is still due to their two screws failing by shear following a displacement-controlled failure check. Simultaneously with the failure of the screws of Panel 3, both bolts at the top of one of the columns fail by shear and 5 s later both bolts at the bottom of the same columns fail by tension, which in turn flags the failure of the complete facade.

Note that in the short time window of the simulation of 100 s, pyrolysis is limited to certain zones of the panel and for limited depths, as shown in Fig. 14 on the complete right. Nevertheless, due to the endothermic process, the pyrolysis reduces temperatures of the inner faces and so expansion and bending of the panels, and consequently results in smaller displacements of the connections. The critical displacement, indicated by the line "Failure", is as such reached later. As this paper focuses on pyrolysis, in the next section connection and panel failures will be neglected, and pyrolysis within the system will be studied for a prolonged time.

#### 5.3. Prolonged pyrolysis

In this section, the simulation conducted in the previous section is extended to 1800 s, without considering any failures. This effectively makes it an OWC simulation, however, for conciseness this paper does not study the differences between OWC and TWC simulations, for they are covered by other works [41,42]. The results are presented in Fig. 15. At the start of the fire simulation, the compartment contains a normal amount of oxygen, which causes the fire to start aggressively, with the temperature load at the fire-exposed face rising to more than 600 degrees in less than 20 s. For the next 40 s, the fire becomes ventilation controlled and temperatures are reduced to 450 degrees. Differently, thanks to its thermal resistance and capacitance, the temperature of the fire-exposed face in the HT analysis smoothly rises from ambient to 400 degrees in 200 s (curve not shown).

Fig. 15(a) shows the HT analyses, with all contour plots made at 1800 s, at the top surface of Panel 3, in the middle. The two contour plots at the top show the temperatures for simulations with (left) and without (right) pyrolysis taken into account. For the



 $Fig. \ 13. \ \ Simulation \ of \ case \ study \ including \ pyrolysis.$ 

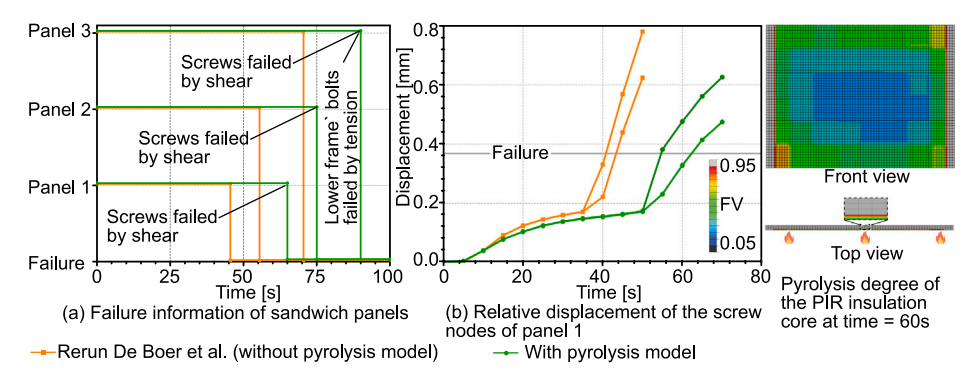


Fig. 14. Panel failures and relative screw displacements for an existing simulation [42] without pyrolysis, and a new simulation including pyrolysis.

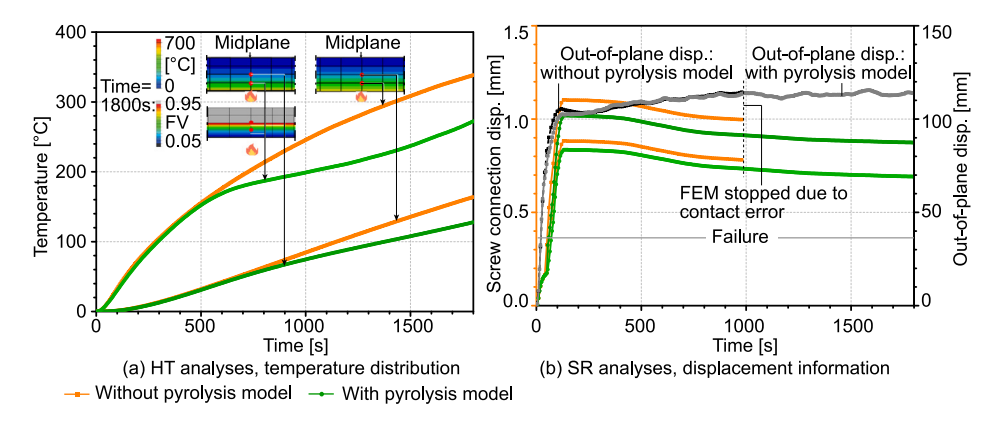


Fig. 15. Results of OWC fire-structure simulations with and without pyrolysis, panel 3. (For interpretation of the references to colour in this figure legend, the reader is referred to the web version of this article.)

simulation with pyrolysis, the single contour plot below shows the pyrolysis degree, with a low Field Variable FV referring to a high degree. For indicated nodes in these contour plots, temperatures over time are given in the graphs. It can be seen that the inclusion of pyrolysis (green lines) delays the heating of the panel compared to the situation without pyrolysis (orange lines). This is more so for locations near the fire, where the pyrolysis degree is higher, i.e. the Field Variable FV is lower. It is difficult to theoretically predict the points at which the temperature curves with and without pyrolysis deviate. First, temperatures are a function of the thermal resistance and capacity in the panel, being themselves functions of the pyrolysis level distribution. For example, the endothermic effects of pyrolysis at the fire-exposed bottom surface only show up later in the middle layer. Second, for pyrolysis at least seven distinct reactions take place between 100 and 900 °C [52], and so it cannot be pinpointed in time in a graph. By the end of the simulation, the pyrolysis level in the first layer of finite elements, measured at 20 mm from the fire, equals about 0.5, and pyrolysis starts in the third layer, 40 mm from the fire. The effect of pyrolysis is significant if it is realised that e.g. for the middle layer it delays a first critical temperature of PIR, 200 °C, see [52], by 10 min.

Fig. 15(b) presents the SR analyses. Due to the thermal expansion of the face (i) the panel bends and so shows out-of-plane displacements, shown in 15(b), following the temperature curve of the fire-exposed face; (ii) the panel screws are loaded in shear due to in-plane expansion. Around 60 s, the shear forces in the screws are so large that the screws become plastic. This allows shear deformations in the screws to become significant, shown in the figure by their linear phase with a relatively high gradient, which also damps out-of-plane deformations due to reverse stress-stiffening. The fire temperature load becomes practically constant after 120 s, which leads to almost constant out-of-plane deformations, and due to thermal relaxation some elastic unloading of the screws. As Fig. 15 shows, pyrolysis does not have a strong influence on the out-of-plane displacements or the relative screw displacements. The somewhat smaller screw displacements, if pyrolysis is included, are possibly due to less thermal expansion, as temperatures are a bit lower, and a reduced stiffness of the partly pyrolysed core. Differences between the two screws are due to the turbulent fire, which leads to zones on the face surface with slightly different temperatures.

It can be concluded that if the failure of connections or panels is not considered, for prolonged fire, significant pyrolysis takes place, which influences the temperature distribution in the interior of the sandwich panel. However, here this only has a marginal effect on the structural behaviour. Note that relatively simple mechanical properties for the PIR core were used in the SR analysis, neglecting factors such as viscoelasticity and delamination. These aspects are important for the prediction of failure related to the panel itself, instead of connection failures, and so should be further investigated in the future.

#### 6. Conclusions and future work

An existing model for 1D pyrolysis has been implemented in the FEM, and verified by an existing model and validated by an existing experiment. The results illustrate how pyrolysis becomes more distributed and less strong over the length in time.

The 1D pyrolysis implementation has been integrated into a 3D FEM, as part of coupled fire-structure simulations. A modification involves the solution of the material decomposition and the integration of the gas mass flux over only one direction of interest, whereas all other operations are 3D. For the applications in this paper, this is possible thanks to the significant difference in size between temperature gradients over the surface and gradients over the thickness of the sandwich panels.

A case study was presented, based on existing literature, making use of fire-structure simulations, and realistic thermal and pyrolysis-related material properties for the PIR insulation core. It was shown that in a short time window of 100 s, pyrolysis is limited to certain zones of the panel and for limited depths. Nevertheless, due to the endothermic process, the pyrolysis reduces temperatures of the inner faces and so expansion and bending of the panels, and consequently results in smaller displacements, and somewhat later failure of the connections.

As this paper focuses on pyrolysis, in a second case, connection failures were neglected, and pyrolysis within the system was studied for a prolonged time. Significant pyrolysis took place, which influenced the temperature distribution in the interior of the sandwich panel. However, there was only a marginal effect on the long-term structural behaviour.

The mechanical properties of the PIR insulation core were assumed as density-dependent, neglecting thermochemical expansion, pore formation, viscoelasticity, and delamination behaviour. However, these aspects are important for the prediction of failure related to the panel itself, instead of connection failures, and so should be further investigated.

Pyrolysis is an important phenomenon to be modelled, also as it may reduce fire risks. Future research can combine pyrolysis with the detailed modelling of bolt [56] and screw [57] connections, using a two-scale method, so that all relevant details of structures can be modelled and investigated for different fire scenarios, including structure to fire effects, supported by experimental validation [49]. These aspects were presented together in a recent PhD thesis by the first author [58]. For future research, it may help that code and scripts to reproduce all the simulations in this paper are available on GitHub [26]. But again, note that the presented model for pyrolysis is only applicable for systems where a significant difference exists in size between gradients over the surface and gradients over the thickness.

#### CRediT authorship contribution statement

Qingfeng Xu: Writing – original draft, Visualization, Software, Methodology, Investigation, Formal analysis, Conceptualization. Hèrm Hofmeyer: Writing – original draft, Supervision, Methodology, Conceptualization. Johan Maljaars: Writing – review & editing, Validation, Supervision. Ruud A.P. van Herpen: Writing – review & editing, Supervision.

#### Declaration of competing interest

The authors declare that they have no known competing financial interests or personal relationships that could have appeared to influence the work reported in this paper.

#### Acknowledgment

The first author was partly financed by the China Scholarship Council (Grant No. 2018-0861-0211), which is highly appreciated.

#### Data availability

All code and scripts to reproduce this research are available on GitHub, as further specified in the paper.

#### References

- A.A. Khan, A.S. Usmani, J.L. Torero, Evolution of fire models for estimating structural fire-resistance, Fire Saf. J. 124 (2021) 103367, http://dx.doi.org/ 10.1016/j.firesaf.2021.103367.
- [2] H.R. Baum, Simulating fire effects on complex building structures, Fire Saf. Sci. 8 (2005) 3-18, http://dx.doi.org/10.3801/IAFSS.FSS.8-3.
- [3] N. Tondini, A. Morbioli, O. Vassart, S. Lechêne, J.-M. Franssen, An integrated modelling strategy between a CFD and an FE software: Methodology and application to compartment fires, J. Struct. Fire Eng. (2016) http://dx.doi.org/10.1108/JSFE-09-2016-015.
- [4] F. Pesavento, M. Pachera, B.A. Schrefler, D. Gawin, A. Witek, Coupled numerical simulation of fire in tunnel, in: AIP Conference Proceedings, Vol. 1922, AIP Publishing LLC, 2018, 090003, http://dx.doi.org/10.1063/1.5019085.
- [5] C. Luo, J. Lua, P.E. DesJardin, Thermo-mechanical damage modeling of polymer matrix sandwich composites in fire, Composites A 43 (5) (2012) 814–821, http://dx.doi.org/10.1016/j.compositesa.2011.03.006, Office of Naval Research (ONR): Composites in Fire.
- [6] C.T. Key, J. Lua, Constituent based analysis of composite materials subjected to fire conditions, Composites A 37 (7) (2006) 1005–1014, http://dx.doi.org/10.1016/j.compositesa.2005.03.022, Special Issue on Fire Behaviour of Composites.
- [7] X. Yan, T. Gernay, Numerical modeling of localized fire exposures on structures using FDS-FEM and simple models, Eng. Struct. 246 (2021) 112997, http://dx.doi.org/10.1016/j.engstruct.2021.112997.
- [8] A.W.G. d'Albani, L.L. de Kluiver, A.C.J. de Korte, R.A.P. van Herpen, R. Weewer, H.J.H. Brouwers, Mass loss and flammability of insulation materials used in sandwich panels during the pre-flashover phase of fire, Fire Mater. 41 (6) (2017) 779–796, http://dx.doi.org/10.1002/fam.2418.
- [9] E.A. Flores-Johnson, Q.M. Li, Experimental study of the indentation of sandwich panels with carbon fibre-reinforced polymer face sheets and polymeric foam core, Composites B 42 (5) (2011) 1212–1219, http://dx.doi.org/10.1016/j.compositesb.2011.02.013.
- [10] M.A. Mousa, N. Uddin, Experimental and analytical study of carbon fiber-reinforced polymer (FRP)/autoclaved aerated concrete (AAC) sandwich panels, Eng. Struct. 31 (10) (2009) 2337–2344, http://dx.doi.org/10.1016/j.engstruct.2009.05.009.
- [11] M.A. Mousa, N. Uddin, Structural behavior and modeling of full-scale composite structural insulated wall panels, Eng. Struct. 41 (2012) 320–334, http://dx.doi.org/10.1016/j.engstruct.2012.03.028.
- [12] A.A. Khan, S. Lin, X. Huang, A.S. Usmani, Facade fire hazards of bench-scale aluminum composite panel with flame-retardant core, Fire Technol. (2021) 1–24, http://dx.doi.org/10.1007/s10694-020-01089-4.
- [13] V. Birman, G.A. Kardomateas, G.J. Simitses, R. Li, Response of a sandwich panel subject to fire or elevated temperature on one of the surfaces, Composites A 37 (7) (2006) 981–988, http://dx.doi.org/10.1016/j.compositesa.2005.03.014, Special Issue on Fire Behaviour of Composites.
- [14] S. Hostikka, A. Matala, Pyrolysis model for predicting the heat release rate of birch wood, Combust. Sci. Technol. 189 (8) (2017) 1373–1393, http://dx.doi.org/10.1080/00102202.2017.1295959.
- [15] V.D. Thi, M. Khelifa, M. Oudjene, M. Ganaoui, Y. Rogaume, Finite element analysis of heat transfer through timber elements exposed to fire, Eng. Struct. 143 (2017) 11–21, http://dx.doi.org/10.1016/j.engstruct.2017.04.014.
- [16] J.B. Henderson, J.A. Wiebelt, M.R. Tant, A model for the thermal response of polymer composite materials with experimental verification, J. Compos. Mater. 19 (6) (1985) 579–595, http://dx.doi.org/10.1177/002199838501900608.
- [17] J.B. Henderson, T.E. Wiecek, A mathematical model to predict the thermal response of decomposing, expanding polymer composites, J. Compos. Mater. 21 (4) (1987) 373–393, http://dx.doi.org/10.1177/002199838702100406.
- [18] Z. Zhang, Thermo-Mechanical Behavior of Polymer Composites Exposed to Fire (Ph.D. thesis), Virginia Polytechnic Institute and State University, USA, 2010.

- [19] H. Li, N. Wang, X. Han, B. Fan, Z. Feng, S. Guo, Simulation of thermal behavior of glass fiber/phenolic composites exposed to heat flux on one side, Materials 13 (2) (2020) 421, http://dx.doi.org/10.3390/ma13020421.
- [20] P.T. Summers, B.Y. Lattimer, S. Case, S. Feih, Predicting compression failure of composite laminates in fire, Composites A 43 (5) (2012) 773–782, http://dx.doi.org/10.1016/j.compositesa.2012.02.003, Office of Naval Research (ONR): Composites in Fire.
- [21] F. Richter, G. Rein, A multiscale model of wood pyrolysis in fire to study the roles of chemistry and heat transfer at the mesoscale, Combust. Flame 216 (2020) 316–325, http://dx.doi.org/10.1016/j.combustflame.2020.02.029.
- [22] K.-Y. Li, X. Huang, C. Fleischmann, G. Rein, J. Ji, Pyrolysis of medium-density fiberboard: optimized search for kinetics scheme and parameters via a genetic algorithm driven by Kissinger's method, Energy Fuels 28 (9) (2014) 6130–6139, http://dx.doi.org/10.1021/ef501380c.
- [23] T.T. Tran, V.-D. Thi, M. Oudjene, M. Khelifa, P. Girods, M. Debal, Y. Rogaume, Y. Jannot, Fire structural performance of thermo-mechanically compressed spruce timber by means experiments and a three-step multi-reactions pyrolysis 3D-finite element modelling, Constr. Build. Mater. 320 (2022) 126100.
- [24] K. Jian, Z.-H. Chen, Q.-S. Ma, W.-W. Zheng, Effects of pyrolysis processes on the microstructures and mechanical properties of Cf/SiC composites using polycarbosilane, Mater. Sci. Eng. A 390 (1) (2005) 154–158.
- [25] M.L. Janssens, Modeling of the thermal degradation of structural wood members exposed to fire, Fire Mater. 28 (2-4) (2004) 199-207.
- [26] Q. Xu, TUe-excellent-buildings/journal\_paper\_pyrolysis\_insulation\_material\_fire\_structure\_simulations: code\_and\_scripts, 2024, http://dx.doi.org/10.5281/zenodo.11400391
- [27] U. Wickström, D. Duthinh, K. McGrattan, Adiabatic surface temperature for calculating heat transfer to fire exposed structures, in: Proceedings of the Eleventh International Interflam Conference. Interscience Communications, London, Vol. 167, 2007, pp. 943–953.
- [28] H.-C. Kung, A mathematical model of wood pyrolysis, Combust. Flame 18 (2) (1972) 185-195, http://dx.doi.org/10.1016/S0010-2180(72)80134-2.
- [29] T.R. Munson, R.J. Spindler, Transient Thermal Behavior of Decomposing Materials. Part 1. General Theory and Application to Convective Heating, Tech. Rep., Avco Corporation. Research and Advanced Development Division, 1961.
- [30] K.J. Laidler, The development of the Arrhenius equation, J. Chem. Educ. 61 (6) (1984) 494.
- [31] C. Lautenberger, C. Fernandez-Pello, Generalized pyrolysis model for combustible solids, Fire Saf. J. 44 (6) (2009) 819-839.
- [32] C. Lautenberger, Gpyro3D: a three dimensional generalized pyrolysis model, Fire Saf. Sci. 11 (2014) 193-207.
- [33] C. Lautenberger, Mapping areas at elevated risk of large-scale structure loss using Monte Carlo simulation and wildland fire modeling, Fire Saf. J. 91 (2017) 768–775.
- [34] C. Lautenberger, C. Fernandez-Pello, Pyrolysis modeling, thermal decomposition, and transport processes in combustible solids, WIT Trans. State Art Sci. Eng. 31 (2008) 209–259.
- [35] A.P. Mouritz, S. Feih, E. Kandare, Z. Mathys, A.G. Gibson, P.E. Des Jardin, S.W. Case, B.Y. Lattimer, Review of fire structural modelling of polymer composites, Composites A 40 (12) (2009) 1800–1814, http://dx.doi.org/10.1016/j.compositesa.2009.09.001.
- [36] D.M. Chaudhari, S.I. Stoliarov, M.W. Beach, K.A. Suryadevara, Polyisocyanurate foam pyrolysis and flame spread modeling, Appl. Sci. 11 (8) (2021) 3463.
- [37] Dassault Systèmes Simulia Corp, ABAQUS Version 6.14, User's Manual, USA, 2014.
- [38] A. Matala, C. Lautenberger, S. Hostikka, Generalized direct method for pyrolysis kinetic parameter estimation and comparison to existing methods, J. Fire Sci. 30 (4) (2012) 339–356.
- [39] K. McGrattan, S. Hostikka, R. McDermott, J. Floyd, C. Weinschenk, K. Overholt, Fire dynamics simulator user's guide, NIST Spec. Publ. 1019 (6) (2013) 1–339.
- [40] N.L. Ryder, J.A. Sutula, C.F. Schemel, A.J. Hamer, V. van Brunt, Consequence modeling using the fire dynamics simulator, J. Hazard. Mater. 115 (1) (2004) 149–154, http://dx.doi.org/10.1016/j.jhazmat.2004.06.018.
- [41] J.A. Feenstra, H. Hofmeyer, R.A.P. van Herpen, M. Mahendran, Automated two-way coupling of CFD fire simulations to thermomechanical FE analyses at the overall structural level, Fire Saf. J. 96 (2018) 165–175, http://dx.doi.org/10.1016/j.firesaf.2017.11.007.
- [42] J.G.G.M. de Boer, H. Hofmeyer, J. Maljaars, R.A.P. van Herpen, Two-way coupled CFD fire and thermomechanical FE analyses of a self-supporting sandwich panel façade system, Fire Saf. J. 105 (2019) 154–168, http://dx.doi.org/10.1016/j.firesaf.2019.02.011.
- [43] J.C.G. Silva, A. Landesmann, F.L.B. Ribeiro, Fire-thermomechanical interface model for performance-based analysis of structures exposed to fire, Fire Saf. J. 83 (2016) 66–78, http://dx.doi.org/10.1016/j.firesaf.2016.04.007.
- [44] J.B. Henderson, J.A. Wiebelt, M.R. Tant, G.R. Moore, A method for the determination of the specific heat and heat of decomposition of composite materials, Thermochim. Acta 57 (2) (1982) 161–171, http://dx.doi.org/10.1016/0040-6031(82)80057-9.
- [45] J.B. Henderson, Y.P. Verma, M.R. Tant, G.R. Moore, Measurement of the thermal conductivity of polymer composites to high temperatures using the line source technique, Polym. Compos. 4 (4) (1983) 219–224, http://dx.doi.org/10.1080/02619180.1982.11753249.
- [46] EN 1999-1-4, Eurocode 9: Design of Aluminium Structures Part 1-4: Cold-Formed Structural Sheeting, European Committee, Brussels, Belgium, 2011.
- [47] EN 14509, Self-Supporting Double Skin Metal Faced Insulated Panels-Factory Made Products-Specifications, European Committee, Brussels, Belgium, 2013.
- [48] EN, 1993-1-8, Eurocode 3: Design of Steel Structures, Part 1-8: Design of Joints, European Committee, Brussels, Belgium, 2005.
- [49] Q. Xu, H. Hofmeyer, J. Maljaars, R.A.P. van Herpen, Full-scale fire resistance testing and two-scale simulations of sandwich panels with connections, Fire Technol. 60 (2024) 2461–2488, http://dx.doi.org/10.1007/s10694-023-01463-y.
- [50] EN 1991-1-2, Eurocode 1: Actions on Structures, Part 1-2: General Actions-Actions on Structures Exposed to Fire, European Committee, Brussels, Belgium, 2012
- [51] EN 1993-1-2, Eurocode 3: Design of Steel Structures, Part 1-2: General Rules-Structural Fire Design, European Committee, Brussels, Belgium, 2005.
- [52] D.M. Marquis, B. Batiot, E. Guillaume, T. Rogaume, Influence of reaction mechanism accuracy on the chemical reactivity prediction of complex charring material in fire condition, J. Anal. Appl. Pyrol. 118 (2016) 231–248, http://dx.doi.org/10.1016/j.jaap.2016.02.007.
- [53] D.M. Chaudhari, S.I. Stoliarov, M.W. Beach, K.A. Suryadevara, Polyisocyanurate foam pyrolysis and flame spread modeling, Appl. Sci. 11 (8) (2021) 3463, http://dx.doi.org/10.3390/appl1083463.
- [54] A. Foster, Understanding, Predicting and Improving the Performance of Foam Filled Sandwich Panels in Large Scale Fire Resistance Tests (Ph.D. thesis), The University of Manchester, UK, 2015.
- [55] EN 1993-1-1, Eurocode 3: Design of steel structures Part 1-1: General rules and rules for buildings., European Committee, Brussels, Belgium, 2005.
- [56] Q. Xu, H. Hofmeyer, J. Maljaars, A two-scale method to include essential behaviour of bolted connections in structures including elevated temperatures, Theor. Appl. Mech. Lett. (2024) http://dx.doi.org/10.1016/j.taml.2024.100526.
- [57] Q. Xu, H. Hofmeyer, J. Maljaars, A two-scale method to include essential screw connection behaviour in two-way coupled fire-structure simulations, J. Struct. Fire Eng. 15 (2) (2024) 247–266, http://dx.doi.org/10.1108/JSFE-01-2023-0005.
- [58] Q. Xu, Simulations of Sandwich Panel Systems under Fire: Two-Scale Methods for Connections, Pyrolysis for Insulation, Experimental Validations (Ph.D. thesis), Eindhoven University of Technology, Department of the Built Environment, Unit Structural Engineering and Design, 2024.